Supporting Information

Growth of Large-Area Graphene Single Crystals in Confined Reaction Space with Diffusion-Driven Chemical Vapor Deposition

Chiao-Chen Chen,[*,†,‡] *Chia-Jung Kuo,*[†] *Chun-Da Liao,*[†] *Chin-Fu Chang,*[†] *Chi-Ang Tseng,*[†] *Chia-Rung Liu*[†] *and Yit-Tsong Chen*[*,†,§]

[†]Department of Chemistry, National Taiwan University
No. 1, Sec. 4, Roosevelt Road
Taipei 106, Taiwan
E-mail: ytcchem@ntu.edu.tw

[‡]Department of Chemistry
Tamkang University
No. 151, Yingzhuan Road
New Taipei City 25137, Taiwan
E-mail: chencc@mail.tku.edu.tw

[§]Institute of Atomic and Molecular Sciences
Academia Sinica
P.O. Box 23-166
Taipei 106, Taiwan

MATERIALS AND METHODS

1. Catalytic growth of graphene

Graphene single crystals were synthesized on a 25-μm-thick Cu foil (Alfa Aesar, purity 99.8%) in an LPCVD chamber. The reaction chamber is composed of a 90-cm-long quartz tube with 2.54 cm in outer diameter and a split-tube furnace (Thermo Scientific, Lindberg/Blue M) with a 10-cm-long heating zone (Figure S1 and 1). For graphene synthesis, the as-received Cu foil was treated with glacial acetic acid (Sigma-Aldrich, ≥99.85%) for 8 hr to remove oxides and contaminations on the Cu surface, followed by thoroughly rinsing with DI water and blow-drying with N_2. The acid-treated Cu foil was then cut into 1 × 2 cm^2 strips and mounted on a tungsten (W) boat to be located in the LPCVD chamber. The tungsten boat was shifted out of the heating zone quickly via a small magnetic dragger after reaction. In the synthetic reaction, the CVD system was first evacuated to ~2 × 10^{-2} torr for 10 min, followed by filling the gas mixture of Ar (FMI Corp., 99.9995%) and H_2 (FMI Corp., 99.9995%). The chamber temperature was then ramped up to 1050 °C within 40 min and kept at 1050 °C (typically for 30 min) for the substrate annealing (Figure S2, Steps I and II). After the annealing, the system temperature was maintained at 1050 °C, followed by introducing CH_4 (FMI Corp., 99.9995%) as the carbon source into the reaction chamber to initiate graphene growth (Figure S2, Step III). After the reaction, while both H_2 and CH_4 flows were turned off, the tungsten boat containing the Cu substrate grown with graphene was quickly shifted out of the hot zone. Finally, the system was cooled to room temperature under an Ar flow (Figure S2, Step IV).

2. Selected oxidation-assisted optical image

To rapidly identify how different synthesis protocols vary the graphene domains produced, we adopted the selective oxidation method, reported by C. Jia and coworkers, which enables the direct optical inspection of the as-grown graphene without going through the laborious transfer process.[S1] With this method, a Cu substrate with the as-grown graphene grains was oxidized in ambient air on a hot plate at 180 °C for 20 min. The graphene film on the Cu substrate could serve as a protection

layer to prevent the underlying Cu surface from oxidation because of its high chemical/thermal stability and impermeability to gases and liquids.[S2, 3] In contrast, the surrounding surface of the Cu foil without being covered by graphene exhibited high reactivity and was readily oxidized to copper oxides with an obvious color change. The apparent color contrast between the oxidized and non-oxidized Cu surfaces made the synthesized graphene domains easy to be observed in an optical microscope (Olympus, BX51) equipped with a charge-coupled device (CCD) camera (Leica, DFC495).

3. Thin-film transfer

For further optical/electrical characterization and device fabrication, the as-grown graphene domains/films on the Cu substrate were transferred onto a p-doped Si wafer with a 300-nm-thick SiO_2 layer or a TEM grid (Electron Microscopy Sciences, LC200-Cu) via a conventional polymer-assisted method.[S4] Because graphene domains/films were grown on both sides of the Cu substrate, we selected one side of the Cu foil (1×1 cm^2) to transfer the as-grown graphene by spin-coating 50 μL of polymethyl methacrylate (MicroChem, 950 PMMA, A4) at 3000 rpm for 30 sec, followed by baking the PMMA/graphene/Cu on a hot plate at 135 °C for 5 min. Meanwhile, the other side of the Cu foil without the PMMA coating was cleaned with O_2 plasma to remove graphene. The plasma cleaned PMMA/graphene/Cu sample was then floated over Marble's solution ($CuSO_4$: HCl : H_2O = 10 g : 50 mL : 50 mL) to etch away the Cu substrate, resulting in a PMMA/graphene membrane suspending on the solution surface. The PMMA/graphene membrane was then transferred to DI water to further remove the remaining etchants and subsequently scooped up with a receiving substrate (a SiO_2/Si wafer or a TEM grid). The PMMA/graphene membrane on the receiving substrate was vacuum dried in a desiccator at room temperature for 2 hr and heated on a hot plate at 85 °C for 15 min to promote the adhesion between graphene and the receiving substrate. The PMMA/graphene/substrate stack was then immersed into acetone at room temperature overnight to remove PMMA, followed by rinsing the graphene/substrate with isopropanol and DI water to

remove organic residues on the graphene surface. Finally, the graphene/substrate was blow-dried with N_2.

4. Device fabrication and electrical measurement

To fabricate filed-effect-transistor (FET) devices, the graphene/substrate was first annealed at 200 ˚C under diluted H_2 flow (H_2 10 sccm/Ar 100 sccm) for 1 hr to remove the remained organic residues during the transfer process. After annealing, selected domains of the graphene/substrate were mounted carefully with a TEM copper grid which served as a shadow mask for the thermal-evaporation deposition of source/drain electrodes (10 nm Cr/50 nm Au). The electrical measurements of the as-fabricated graphene-FET devices were conducted in a probe station (Lakeshore, TTPX) equipped with a source meter (Keithley, 2636A) under the chamber pressure of ~ 2×10^{-3} torr at room temperature. In the measurements, a back gate voltage (V_g) was applied through the p-doped Si substrate with a 300-nm-thick SiO_2 dielectric layer. From the recorded source-drain current vs. source-drain voltage (I_{sd}–V_{sd}) and source-drain current vs. gate voltage (I_{sd}–V_g) curves, the device resistance (R_{tot}), which is composed of the contact resistance ($R_{contact}$) of metal/graphene and the graphene channel resistance ($R_{channel}$), can be determined.[S5, 6]

$$R_{tot} = \frac{V_{sd}}{I_{sd}} = R_{contact} + R_{channel} = R_{contact} + \frac{L}{W} \cdot \rho \quad \text{(S1)}$$

In Equation S1, L refers to the channel length between the source and drain electrodes, W is the channel width, and ρ denotes the channel resistivity of the graphene-FET device. In addition, the conductivity ($\sigma = 1/\rho$) of the graphene channel is related to filed-effect mobility (μ_{EF}), elementary charge (e), and carrier density (n) as shown in Equation S2.[S6]

$$\rho = \sigma^{-1} = (ne\mu_{EF})^{-1} = \left(\mu_{\mathrm{EF}} \sqrt{e^2 n_0^2 + \left[C_g \left(V_g - V_{Dirac} \right) \right]^2} \right)^{-1} \quad \text{(S2)}$$

In Equation S2, n_0 is the residual carrier density at the Dirac point due to charged impurity, C_g is the capacitance per unit area of the gate dielectric, and V_{Dirac} refers to the recorded potential shift at the Dirac point. The combination of Equation S1 and S2 yields Equation S3, in which R_{tot} is

represented as a function of V_g–V_{Dirac}. It is noted that $R_{contact}$ can be determined from Equation S3 by fitting the recorded data of R_{tot} and V_g–V_{Dirac}.[S7]

$$R_{tot} = \frac{V_{sd}}{I_{sd}} = R_{contact} + \frac{L}{W} \cdot \rho$$

$$= R_{contact} + \frac{L}{W} \cdot \frac{1}{\mu_{EF}\sqrt{e^2 n_0^2 + \left[C_g\left(V_g - V_{Dirac}\right)\right]^2}}$$

$$= R_{contact} + \frac{L}{W} \cdot \frac{1}{n_0 e \mu_{EF}}\left[1 + \frac{C_g^2}{n_0^2 e^2}\left(V_g - V_{Dirac}\right)^2\right]^{-1/2} \quad \text{(S3)}$$

5. FEM simulation of the flow field in confined reaction space

Two COMSOL Multiphysics modules in the finite element model (FEM), i.e., laminar flow (Navier-Stokes equation) and transport of dilute species (convection-diffusion equation), were coupled to solve the flow field and mass transport of the reactants flow involved in our CVD reaction. Simulations were performed with a commercial FEM package of COMSOL Multiphysics (version 4.4). The three-dimensional geometry shown in Figure S1a describes the CVD reaction system used in this study for graphene synthesis. This system consists of a quartz tube (2.54 cm/2.15 cm in outer/inner diameter and 90 cm in length) with a rectangular reactor (L 25 mm × W 18 mm × H 4 mm) located in the center. Within the rectangular reactor, a confined reaction room (L 22 mm × W 13 mm × H 50 μm) with one open end (as an inlet) was designed to allow the insertion of a 25-μm-thick Cu foil and the entry of reacting gases. It is noteworthy that the inlet was oriented towards tailwind to prevent the direct injection of gas flow. To save the memory space required in computation and to facilitate the illustration of simulated results, a reduced three-dimensional geometry with a plane of symmetry (Figure S1b) was utilized for the FEM simulations. In addition, the graphene synthesis was conducted in the heating zone located within the central 10-cm-long region of the quartz tube (Figure 1 and S1). Therefore, our discussion about the simulated flow fields and mass transports is focused on this region (Figure S1c). In this simulation, the flow was

considered as a gas mixture of CH_4, H_2, and Ar with a constant inlet speed consistent with the experimental conditions. In addition, to demonstrate the scalability of the CVD method adopted in this study, a simulation for the CVD reaction system composed of a large tube furnace (Figure S6a–c, 20.32 cm in diameter and 120 cm in length, adapted from the chamber dimensions reported by Bae, S. et. al., *Nat. Nanotechnol.*, **2010**, *5*, 574-578)[S8] with an amplified rectangular reactor (Figure S6d, L 20 cm × W 14.4 cm × H 4 mm containing a confined reaction room of L 17.6 cm × W 10.4 cm × H 50 μm) was performed.

6. Estimation of boundary layer thickness

Over a flat plane, the boundary layer thickness (δ) can be estimated with the following equation:[S9, 10]

$$\delta = 4.91\sqrt{\frac{\nu x}{U}} \qquad \text{(S4)}$$

where ν refers to the kinematic viscosity (m^2/s), x is the distance downstream from the start of the boundary layer (m) and U is the free stream velocity (m/s). In the LPCVD system at 1050 ˚C and 1.71 torr, the kinematic viscosity of $\nu \sim 1 \times 10^{-2}$ m^2/s was estimated for the reactant mixture (i.e., H_2, CH_4, and Ar).[S11] The free stream velocity (U) at the entrance of the confined reaction space is $\sim 1 \times 10^{-2}$ m/s obtained from the FEM simulation. Since the Cu substrate was located typically at ~1 mm away from the entrance of the confined reaction space, the distance from the start of the boundary (x) was assumed to be 10^{-3} m in the calculation. From the calculation with Equation S4,

$$\delta = 4.91\sqrt{\frac{\nu x}{U}} = 4.91\sqrt{\frac{10^{-2} \times 10^{-3}}{10^{-2}}} = 0.16 \text{ m} = 16 \text{ cm}.$$

Since the height of the confined reaction room to accommodate the catalytic Cu substrate is only 50 μm, the boundary layer is believed to extend over the entire space between the Cu surface and quartz slides.

Table S1. Synthesis protocols utilized in this study

Protocol	Temp	Annealing step				Growing step					Reactor type	Grain size	Grain density
	(˚C)	Pressure (torr)	Ar (sccm)	H_2	Time (min)	Pressure (torr)	Ar (sccm)	H_2	CH_4	Time (min)		(μm)	(nuclei/cm^2)
P1	1050	1.04	200	50	60	0.18	0	25	1	20	on W boat	~15	~9.6E+5
P2	1050	1.04	200	50	60	0.18	0	25	1	90	sandwiched between quartz slides	~50	~6.8E+4
P3	1050	1.04	200	50	60	3.43	1000	25	1	25	Confined space	~20	~4.7E+4
P4	1050	1.03	200	10	60	1.71	500	22	1	60		~100	~1.2E+4
P5	1050	1.67	500	10	60	1.71	500	22	1	100		~150	~8.7E+3
P6	1050	2.45	1000	10	60	1.71	500	22	1	105		~200	~5.7E+3
P7	1050	3.12	1500	10	60	1.71	500	22	1	135		~250	~4.4E+3
P8	1050	3.69	2000	10	60	1.71	500	22	1	155	Confined space	~300	~2.8E+3
P9	1050	3.12	1500	10	30	1.71	500	22	1	165		~300	~4.0E+3
P10	1050	3.69	2000	10	30	1.71	500	22	1	180		~350	~2.5E+3
P11	1050	3.67	2000	8	30	1.71	500	22	1	240		~550	~6.3E+2
P12	1050	3.65	2000	5	30	1.71	500	22	1	270		~800	~2.1E+2
P13	1050	3.69	1500	10	60	1.30	330	28	1	120		~180*	~8.2E+2*

*These results are obtained using the reactor with a gap size of 50 μm.

Table S2. Performance parameters of representative protocols for the synthesis of large graphene single crystals.

Ref.	Maximum Grain size (mm)	Averaged growth rate (μm/min)	Duration of a synthesis cycle to obtain 0.8 mm graphene grain* (min)	Electrical mobility ($cm^2V^{-1}s^{-1}$)	Required highest temperature (°C)
12	10	13.9	90	15000~30000	1035
13	0.5†	6	N. A.	4000	1035
14	2	5.6	160	5200	1035
15	1.1	3.6	340	N. A.	1100
16	2.3	18.4	460	11000	1077
17	5	2.1	400	16000	1070
20	0.61	22	N. A.	N. A.	1045
21	0.1	3.3	N. A.	4200	1000
22	1.2	4	320	2440	1050
This work	0.84	3.1	300	4800	1050

*Duration of a synthesis cycle includes the annealing and growth periods to obtain a graphene grain with 0.8 mm in diameter.

†Performance parameters that are less superior or comparable to this work are marked with shading for easier comparison.

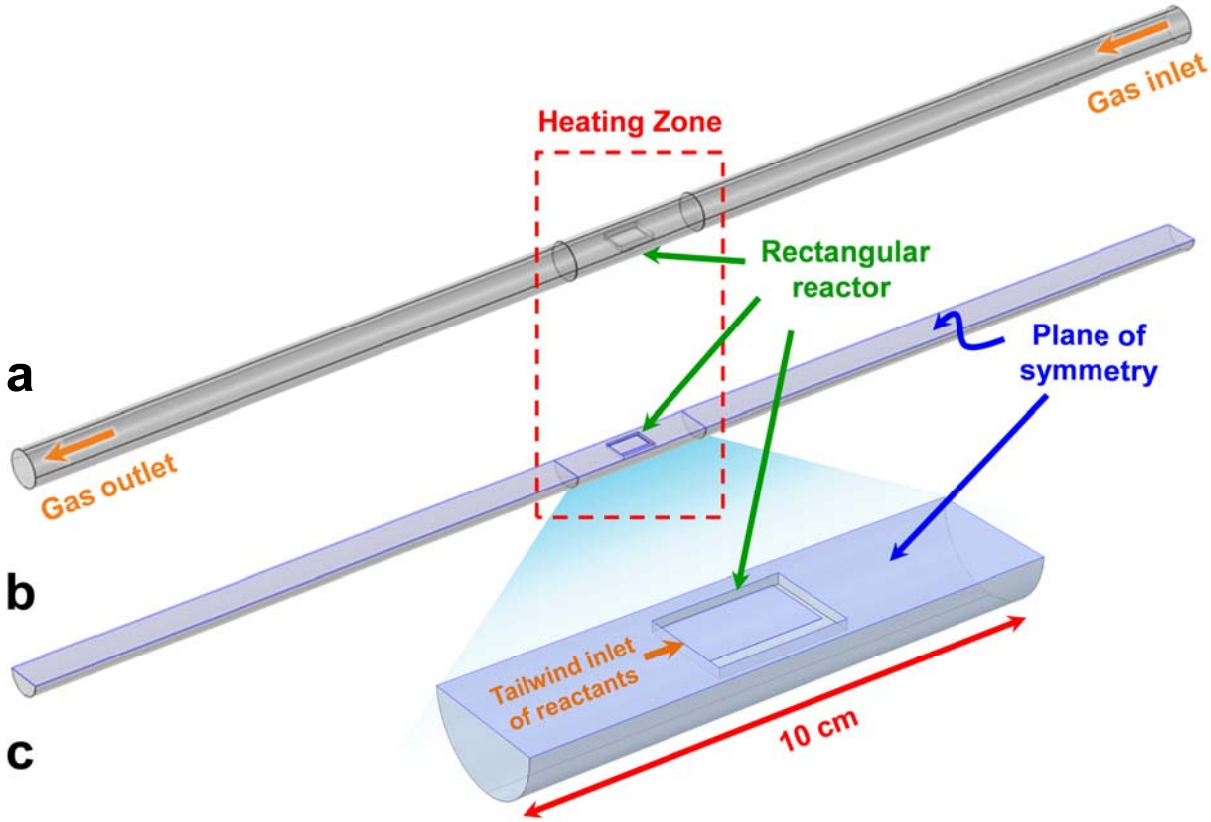

Figure S1. (a) The three-dimensional geometry of the CVD system utilized in this study. This system consists of a quartz tube (2.54 cm/2.15 cm in outer/inner diameter and 90 cm in length) and a rectangular reactor (L 25 mm × W 18 mm × H 4 mm) located in the central 10-cm-long heating zone. A confined reaction space (L 22 mm × W 13 mm × H 50 μm) with one open end (as an inlet) was designed to allow the insertion of a 25-μm-thick Cu foil and the entry of reacting gases. The inlet of reacting gases was oriented towards tailwind to prevent the direct injection of gas flow. (b) The reduced three-dimensional geometry of (a) with a plane of symmetry utilized in the FEM simulations. (c) An enlarged diagram of (b) with an emphasis on the 10-cm-long heating zone.

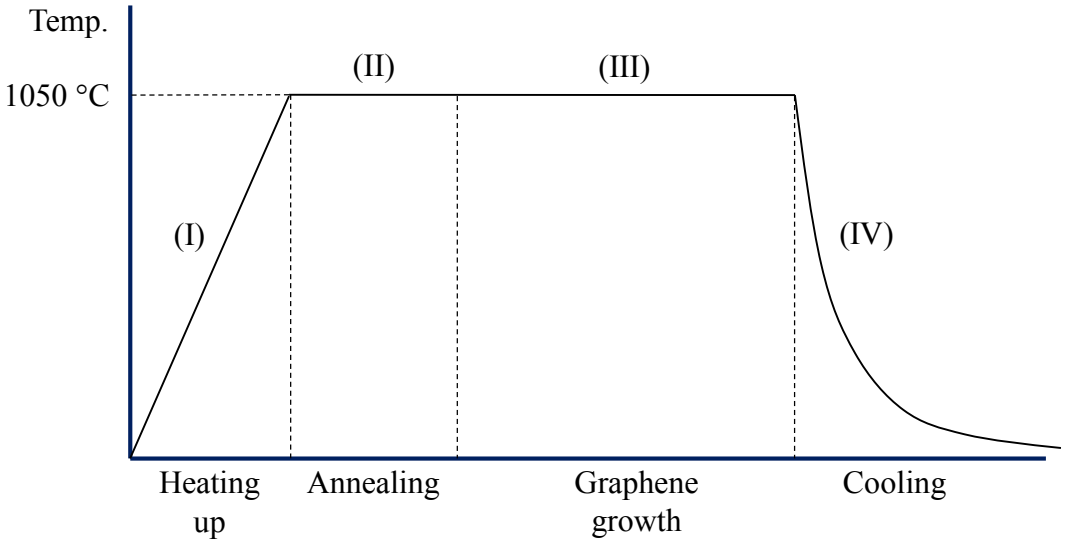

Figure S2. A workflow diagram for the graphene synthesis in LPCVD reaction employed in this study. Experimental details for the chamber pressure, flow rate of each reacting gas, and elapsed reaction time involved in the annealing and growing stages are tabulated in Table S1. In all tests, the ramp-up time for the chamber temperature, from 25 to 1050 ˚C, at the heating-up stage was 40 min.

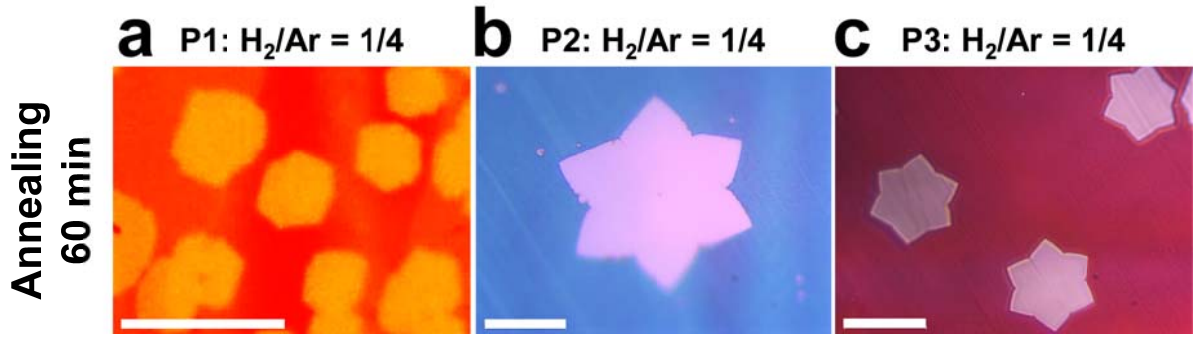

Figure S3. Enlarged optical micrographs of the as-synthesized graphene grains shown in Figure 2d–f for easier comparison of the graphene-shape transformation due to different growth-controlling mechanisms, i.e., surface-reaction (edge-attachment) versus mass-transport (diffusion). Scale bars: 20 μm.

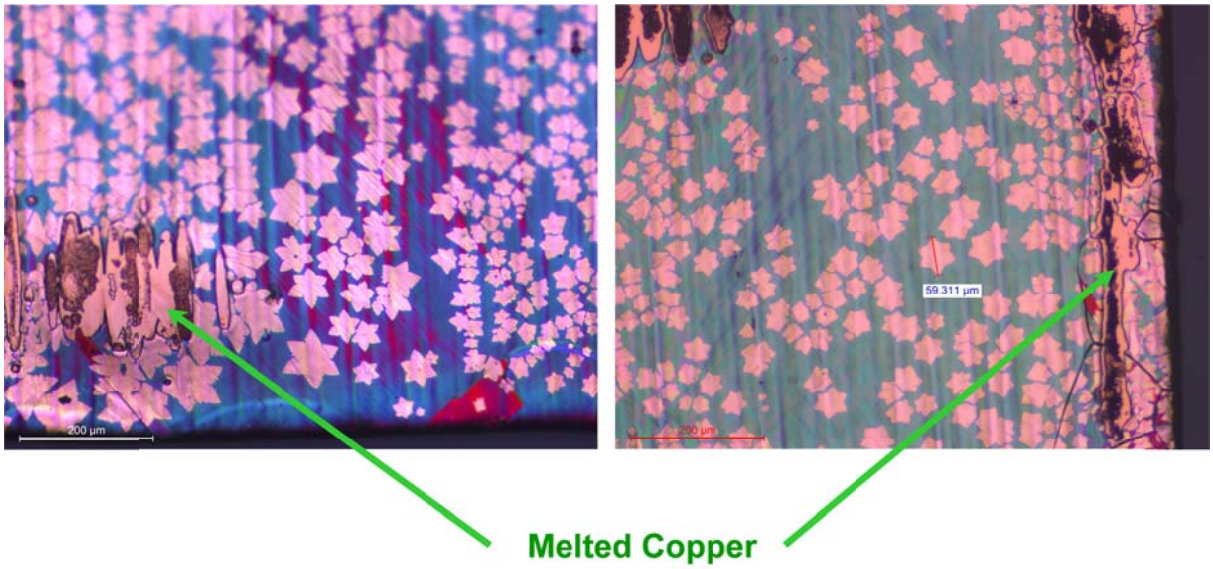

Figure S4. Parts of the Cu substrate melted at elevated temperature to coalesce with the reactor, making it difficult to remove the as-grown graphene/Cu substrate from quartz slides after the reaction for further optical characterization and device fabrication.

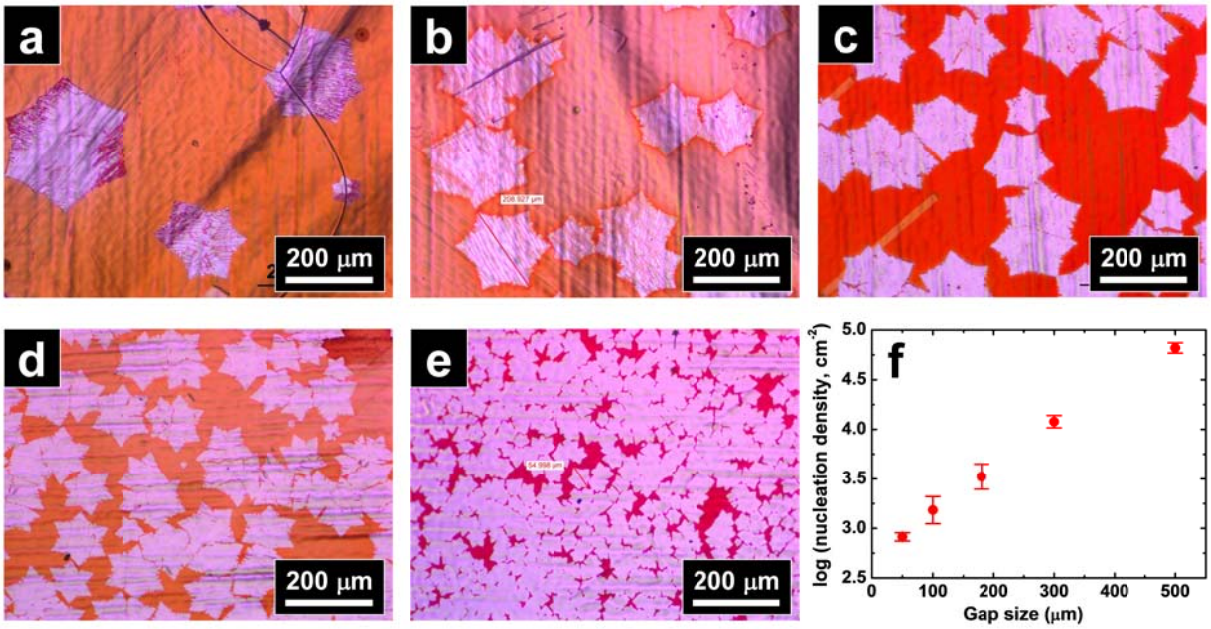

Figure S5. With the same synthesis protocol (Table S1, P13), graphene samples obtained from five reactors of different gap sizes, (a) 50 μm, (b) 100 μm, (c) 180 μm, (d) 300 μm, and (e) 500 μm, were investigated to find the optimal gap size for a 25-μm-thick Cu catalytic foil. (f) The resultant nucleation density decreases monotonically with the reduction of gap size.

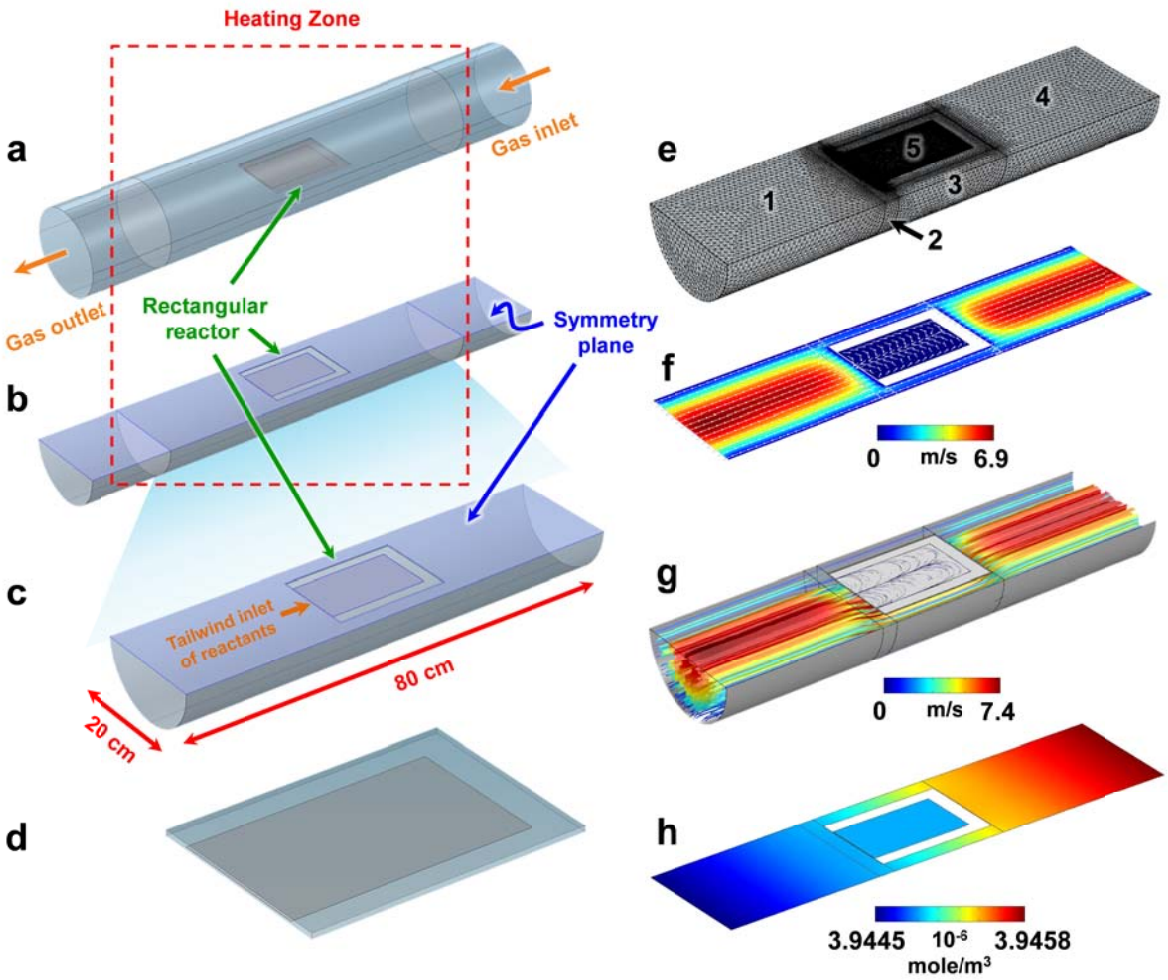

Figure S6. (a–b) The three-dimensional geometry of an enlarged CVD system composed of a quartz tube (20.32 cm in outer diameter and 120 cm in length) with a rectangular reactor (L 20 cm × W 14.4 cm × H 4 mm) located in the central heating zone of 80 cm in length. (c) The reduced three-dimensional geometry of (a) with a plane of symmetry utilized in the FEM simulation. The inlet of reacting gases was also oriented towards tailwind to prevent the direct injection of gas flow. (d) The zoom-in geometry of the rectangular reactor with a confined reaction space of L 17.6 cm × W 10.4 cm × H 50 μm. (e) The meshed geometry of (c) illustrates that different domains were meshed with different space resolutions to achieve the most efficient simulation. The simulation results of this enlarged CVD system show that the fluid conditions, including (f) reduced flow velocity, (g) diffusion-dominant fluxes, and (h) a homogenous reactant distribution, are similar to those (shown in Figure 1) of the chamber/reactor with much smaller dimensions.

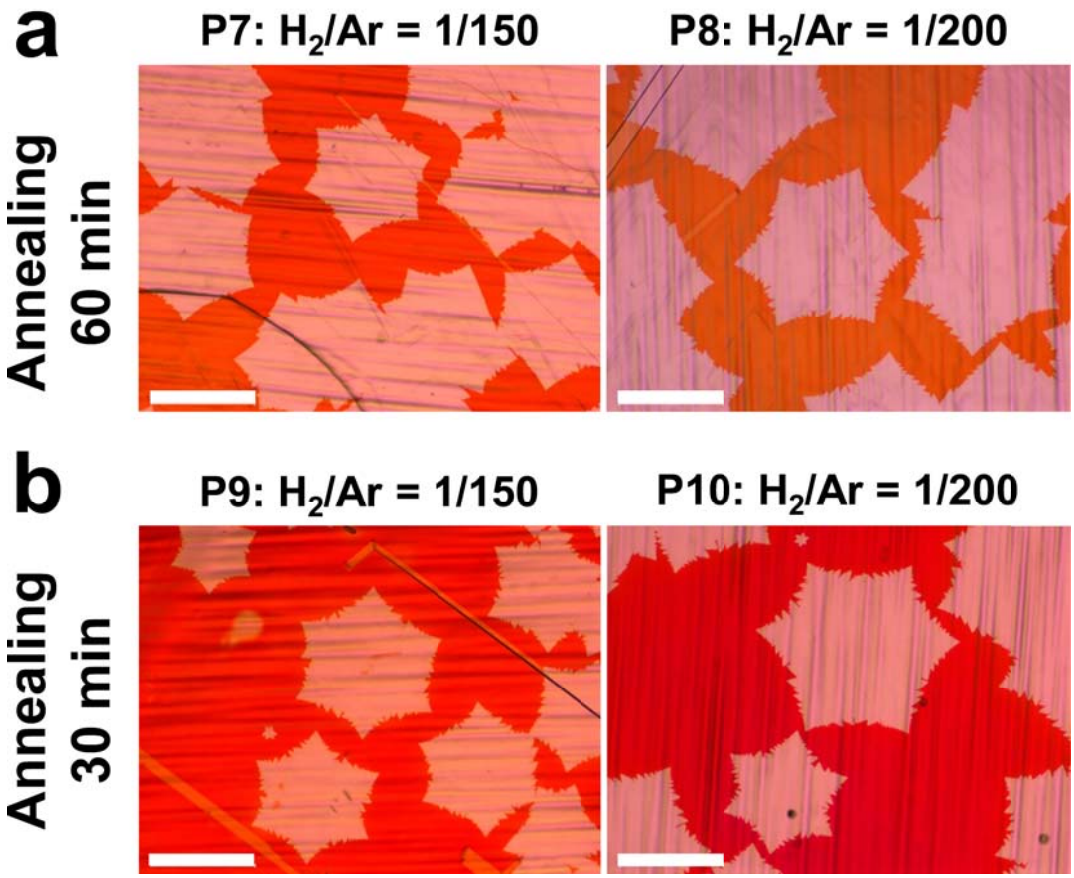

Figure S7. Comparison of the as-grown graphene grains from the same synthesis protocols except the H_2 exposure time during annealing. These results demonstrate that, apart from the reduction of H_2 concentration, the shortened exposure time to H_2 during annealing further lessens the nucleation density. Scale bars: 200 μm.

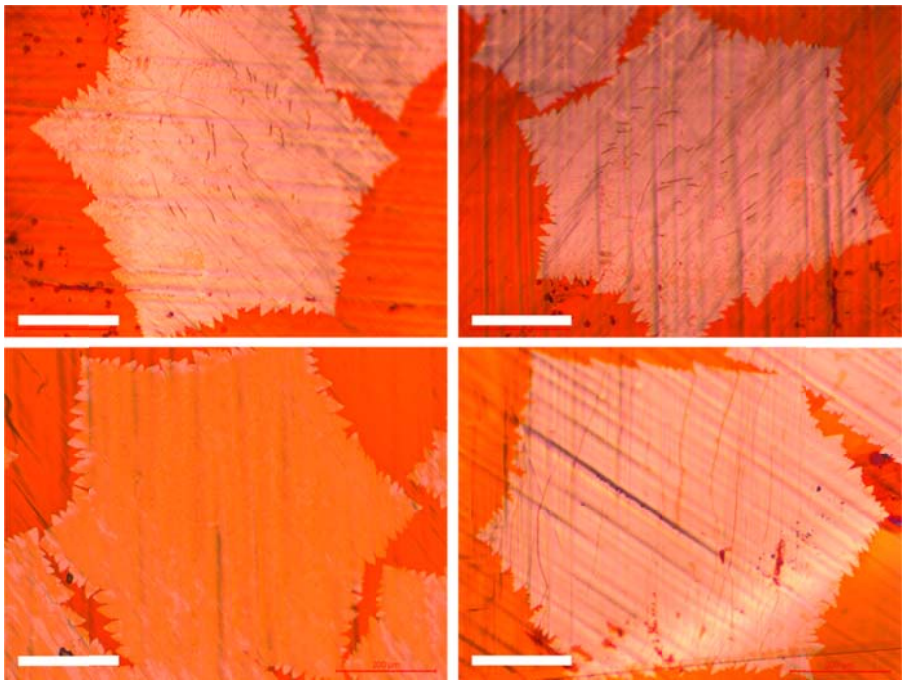

Figure S8. Representative examples of the large-area graphene single crystals synthesized from different experimental batches with the optimized synthesis protocol of P12. Scale bars: 200 μm.

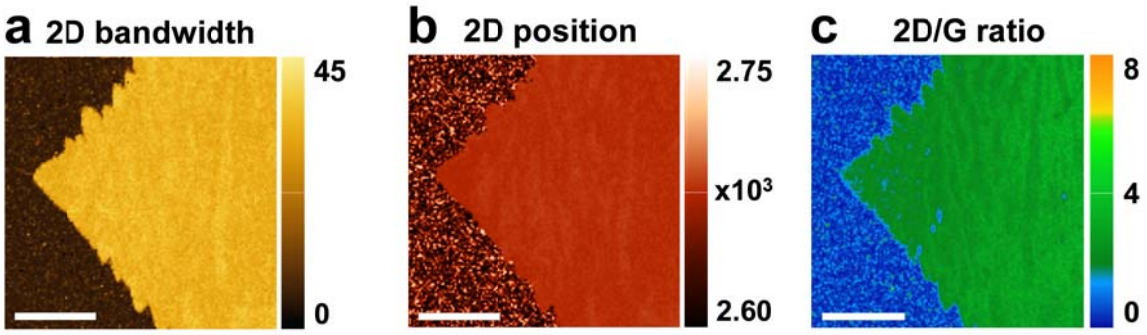

Figure S9. Raman mappings of the 2D bandwidth (FWHM), 2D peak position, and intensity ratio of I_{2D}/I_G collected from the selected area marked by a red-dashed square in Figure 4a. Scale bars: 30 μm.

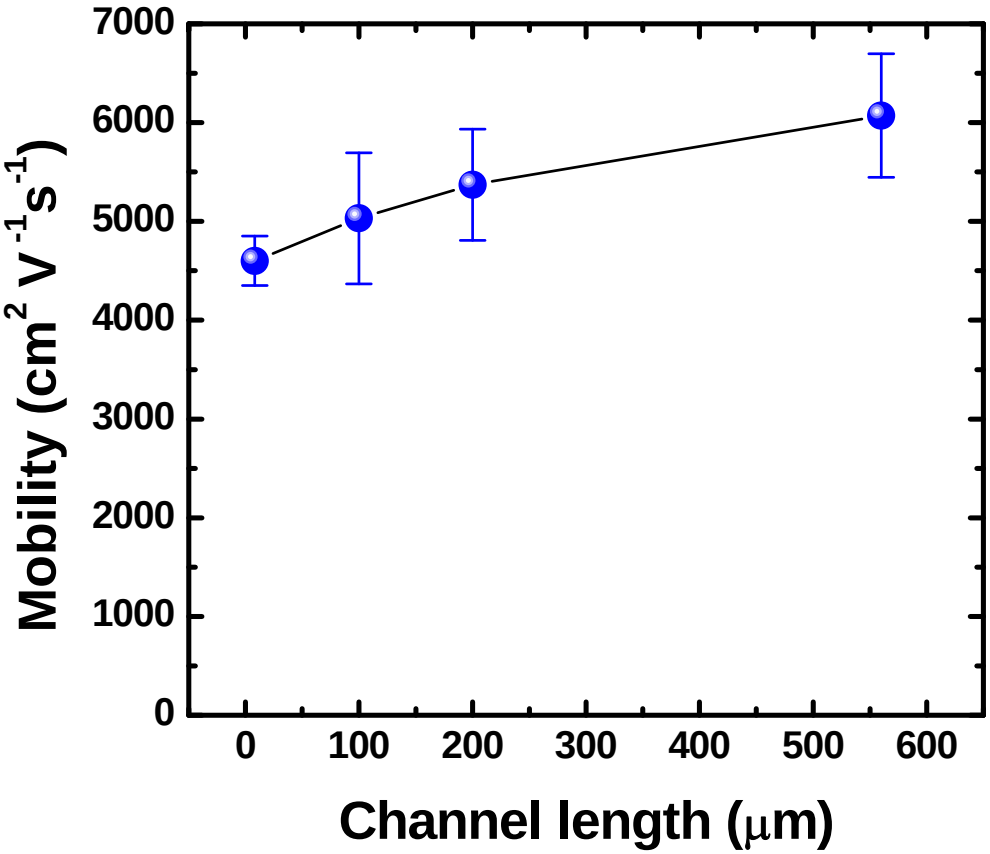

Figure S10. The electrical measurements show that the field-effect mobility of graphene devices is dependent on the channel length (L_{ch}) ranging from 8, 100, 200, to 560 μm, where the channel width (W_{ch}) of the graphene devices was maintained to be >50 μm to minimize the effect of width-dependent mobility.

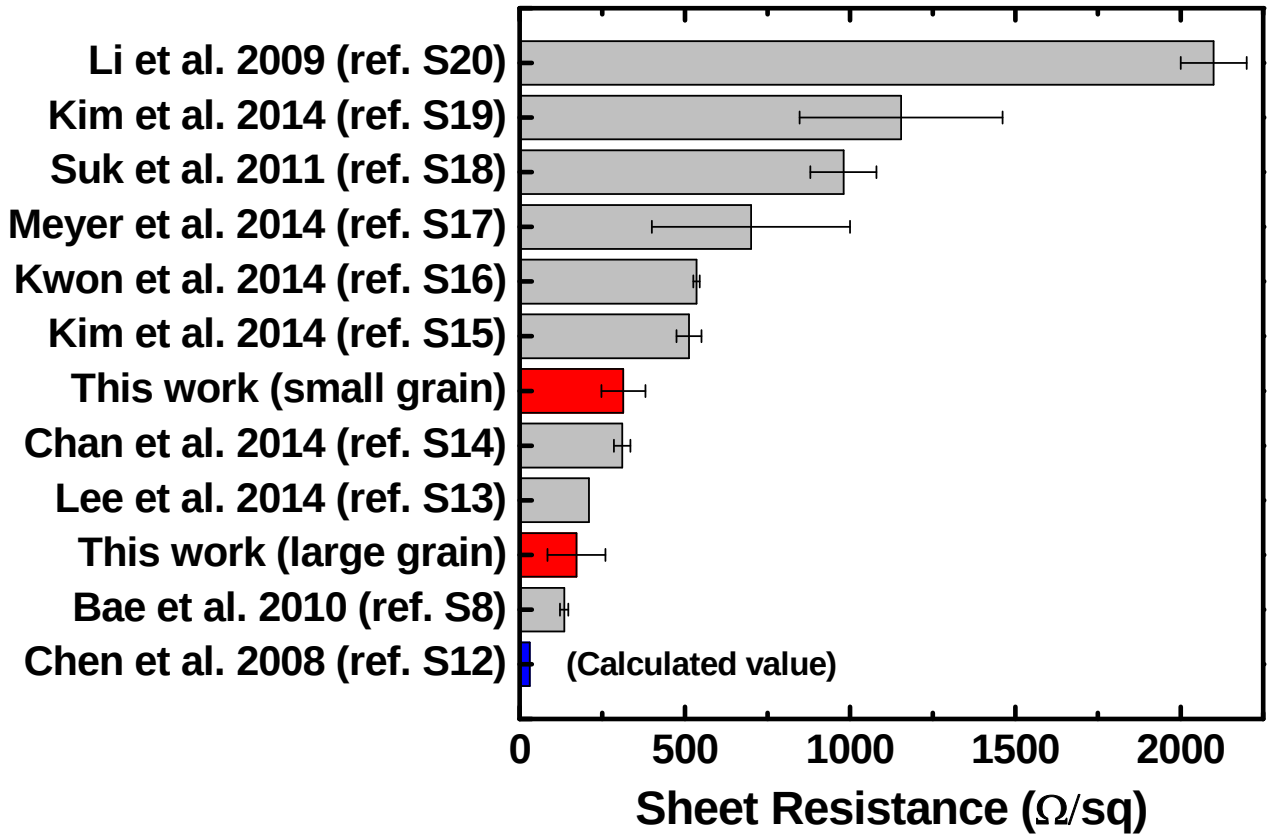

Figure S11. Comparison of the sheet resistances of several pristine CVD-synthesized monolayer graphene films. While the intrinsic sheet resistance of graphene is estimated to be ~30 Ω/sq as indicated with a blue bar,[S12] the sheet resistances reported recently by several representative groups are illustrated with gray bars.[S8, 13-20] For the continuous graphene films prepared in this study (marked by red), the sheet resistances are determined to be 171.9 ± 87.4 Ω/sq for the graphene films composed of multiple large graphene single crystals and 367.7 ± 120.5 Ω/sq for those films that consist of multiple small graphene grains.

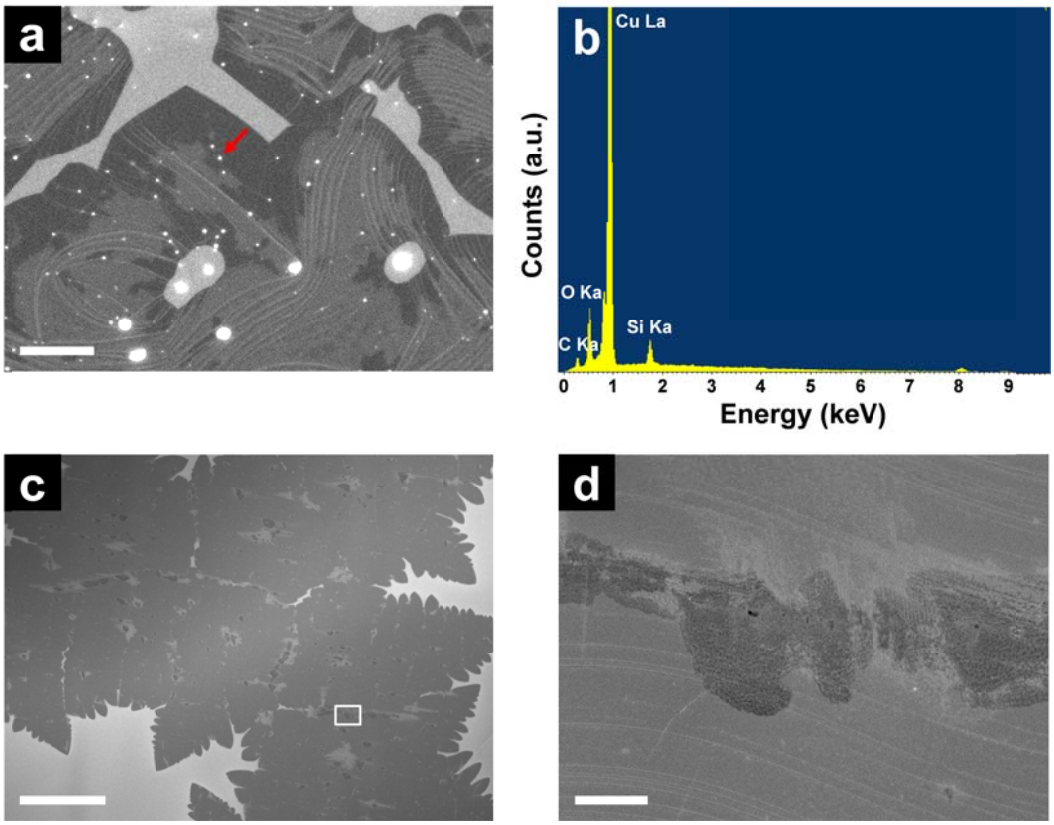

Figure S12. (a) An SEM image shows the significant contamination of SiO_2 nanoparticles (small white dots) on the as-grown graphene on a Cu substrate, which was obtained from a conventional CVD reaction (Figure 2a). (b) The nanoparticle, marked with a red arrow in (a), was analyzed by energy-dispersive X-ray spectroscopy (EDS) to comprise silicon and oxygen, resulting from the H_2 etching of a quartz tube in the graphene synthesis. (c) In sharp contrast, the as-grown graphene synthesized within a confined reaction room (Figure 2c) is free of SiO_2 contamination. (d) A zoom-in image of the area marked with a white square in (c) further confirms the cleanness of the graphene surface. Scale bars: (a) 2 μm, (c) 40 μm, and (d) 2 μm.

Reference

S1. Jia, C.; Jiang, J.; Gan, L.; Guo, X. Direct Optical Characterization of Graphene Growth and Domains on Growth Substrates. *Sci. Rep.*, **2012**, *2*, 707.

S2. Bunch, J. S.; Verbridge, S. S.; Alden, J. S.; van der Zande, A. M.; Parpia, J. M.; Craighead, H. G.; McEuen, P. L. Impermeable Atomic Membranes from Graphene Sheets. *Nano Lett.*, **2008**, *8*, 2458-2462.

S3. Su, Y.; Kravets, V. G.; Wong, S. L.; Waters, J.; Geim, A. K.; Nair, R. R. Impermeable Barrier Films and Protective Coatings Based on Reduced Graphene Oxide. *Nat. Commun.*, **2014**, *5*, 4843.

S4. Kang, J.; Shin, D.; Bae, S.; Hong, B. H. Graphene Transfer: Key for Applications. *Nanoscale*, **2012**, *4*, 5527-5537.

S5. Kim, S.; Nah, J.; Jo, I.; Shahrjerdi, D.; Colombo, L.; Yao, Z.; Tutuc, E.; Banerjee, S. K. Realization of a High Mobility Dual-Gated Graphene Field-Effect Transistor with Al_2O_3 Dielectric. *Appl. Phys. Lett.*, **2009**, *94*, 062107.

S6. Liao, L.; Bai, J.; Qu, Y.; Lin, Y.-c.; Li, Y.; Huang, Y.; Duan, X. High-κ Oxide Nanoribbons as Gate Dielectrics for High Mobility Top-Gated Graphene Transistors. *Proc. Natl. Acad. Sci. USA*, **2010**, *107*, 6711-6715.

S7. Liu, L.; Zhou, H.; Cheng, R.; Yu, W. J.; Liu, Y.; Chen, Y.; Shaw, J.; Zhong, X.; Huang, Y.; Duan, X. High-Yield Chemical Vapor Deposition Growth of High-Quality Large-Area AB-Stacked Bilayer Graphene. *ACS Nano*, **2012**, *6*, 8241-8249.

S8. Bae, S.; Kim, H.; Lee, Y.; Xu, X.; Park, J.-S.; Zheng, Y.; Balakrishnan, J.; Lei, T.; Ri Kim, H.; Song, Y. I.; Kim, Y.-J.; Kim, K. S.; Ozyilmaz, B.; Ahn, J.-H.; Hong, B. H.; Iijima, S. Roll-to-Roll Production of 30-inch Graphene Films for Transparent Electrodes. *Nat. Nanotechnol.*, **2010**, *5*, 574-578.

S9. Blasius, H. Grenzschichten in Flüssigkeiten mit kleiner Reibung. *Z. Math. Phys.*, **1908**, *56*, 1-37.

S10. Rubin, H., *Environmental Fluid Mechanics*, CRC Press: Florida, USA, 2001; pp 251-258.

S11. Wallard, A.; Sené, M.; Craston, D.; Williams, J.; Milton, M., *Tables of Physical & Chemical Constants*, Kaye & Laby Online, http://www.kayelaby.npl.co.uk/general_physics/2_2/2_2_3.html, Accessed March 15, 2015.

S12. Chen, J.-H.; Jang, C.; Xiao, S.; Ishigami, M.; Fuhrer, M. S. Intrinsic and Extrinsic Performance Limits of Graphene Devices on SiO_2. *Nat. Nanotechnol.*, **2008**, *3*, 206-209.

S13. Lee, D.; Kwon, G. D.; Kim, J. H.; Moyen, E.; Lee, Y. H.; Baik, S.; Pribat, D. Significant Enhancement of the Electrical Transport Properties of Graphene Films by Controlling the Surface Roughness of Cu Foils Before and During Chemical Vapor Deposition. *Nanoscale*, **2014**, *6*, 12943-12951.

S14. Chan, S.-H.; Chen, J.-W.; Chen, H.-P.; Wei, H.-S.; Li, M.-C.; Chen, S.-H.; Lee, C.-C.; Kuo, C.-C. The Deviation of Growth Model for Transparent Conductive Graphene. *Nanoscale Res. Lett.*, **2014**, *9*, 581.

S15. Kim, H.; Bae, S.-H.; Han, T.-H.; Lim, K.-G.; Ahn, J.-H.; Lee, T.-W. Organic Solar Cells Using CVD-Grown Graphene Electrodes. *Nanotechnology*, **2014**, *25*, 014012.

S16. Kwon, K. C.; Ham, J.; Kim, S.; Lee, J.-L.; Kim, S. Y. Eco-Friendly Graphene Synthesis on Cu Foil Electroplated by Reusing Cu Etchants. *Sci. Rep.*, **2014**, *4*, 4830.

S17. Meyer, J.; Kidambi, P. R.; Bayer, B. C.; Weijtens, C.; Kuhn, A.; Centeno, A.; Pesquera, A.; Zurutuza, A.; Robertson, J.; Hofmann, S. Metal Oxide Induced Charge Transfer Doping and Band Alignment of Graphene Electrodes for Efficient Organic Light Emitting Diodes. *Sci. Rep.*, **2014**, *4*, 5380.

S18. Suk, J. W.; Kitt, A.; Magnuson, C. W.; Hao, Y.; Ahmed, S.; An, J.; Swan, A. K.; Goldberg, B. B.; Ruoff, R. S. Transfer of CVD-Grown Monolayer Graphene onto Arbitrary Substrates. *ACS Nano*, **2011**, *5*, 6916-6924.

S19. Kim, K.; Lee, H.-B.-R.; Johnson, R. W.; Tanskanen, J. T.; Liu, N.; Kim, M.-G.; Pang, C.; Ahn, C.; Bent, S. F.; Bao, Z. Selective Metal Deposition at Graphene Line Defects by

Atomic Layer Deposition. *Nat. Commun.*, **2014**, *5*, 4781.

S20. Li, X.; Zhu, Y.; Cai, W.; Borysiak, M.; Han, B.; Chen, D.; Piner, R. D.; Colombo, L.; Ruoff, R. S. Transfer of Large-Area Graphene Films for High-Performance Transparent Conductive Electrodes. *Nano Lett.*, **2009**, *9*, 4359-4363.